J. Electroanal. Chem., 351 (1993) 65–79
Elsevier Sequoia S.A., Lausanne
JEC 02609

Semi-empirical calculations of the vibrational frequency of carbon monoxide adsorbed on noble metal single-crystal surfaces

P.A. Paredes Olivera and E.P.M. Leiva

Unidad Docente de Matemática, Facultad de Ciencias Químicas, Universidad Nacional de Córdoba, Sucursal 16, Casilla de Correo 61, 5016 Córdoba (Argentina)

E.A. Castro and A.J. Arvía

INIFTA, Facultad de Ciencias Exactas, Universidad Nacional de la Plata, Sucursal 4, Casilla de Correo 16, 1900 La Plata (Argentina)

(Received 24 January 1992; in revised form 21 September 1992)

Abstract

In this work we perform a theoretical analysis of the shift of the observed IR reflection–absorption spectroscopy (IRRAS) band of CO adsorbed on Pt(111), Rh(111) and Pt(100) single crystals as a function of both the degree of CO surface coverage and the electric potential applied at either the metal–vacuum or the metal–solution interface.

The wavefunctions obtained using a modified extended Hückel molecular orbital (EHMO) method are used to predict the vibrational frequency data. The Pt(110), Rh(111) and Pt(111) single crystals are modelled by bilayer clusters of 25 and 22 atoms respectively. A theoretical description of the observed IRRAS shift is analysed by means of a population analysis of CO molecular orbitals, which confirms the donation–back-donation model.

INTRODUCTION

The chemisorption of CO on noble metals such as Pt and Rh in aqueous solution is of particular interest in relation to C1 chemistry [1–6] because CO acts as a poison in the catalytic electro-oxidation of a number of organic compounds such as methanol, formic acid and hydrocarbons through the occupancy of substrate active surface sites [7,8]. The possibility of improving this situation has encouraged research work aimed at obtaining a better understanding of the metal–CO bond and the adsorbed CO electro-oxidation mechanism.

The electro-oxidation mechanism of CO adsorbed on Pt and Rh low Miller indexed surfaces has recently been interpreted at the atomic level in terms of

co-operative interactions between CO and OH adsorbed in vicinal substrate sites through the semi-empirical approach [9,10].

The use of vibrational spectroscopic probes to characterize small adsorbates at ordered monolayer surfaces in an ultrahigh vacuum (UHV) provides valuable structural information about surface systems, and in this respect the application of IR reflection–absorption spectroscopy (IRRAS) to metal–solution interfaces involving well-ordered single crystals provides an opportunity for in-situ characterization of these systems [11–14].

The shifts in the vibrational spectra of some adsorbates in UHV and in the electrochemical environment have been related to the influence of the solution phase on the adsorption process [15,16].

Different approaches can be used to predict the shift of the frequency of the C–O internal mode for CO adsorbed on transition metal surfaces [17–24]. For instance, the use of the extended Hückel molecular orbital method (EHMO) has been employed to study the stability of CO, H and O on Ni(111) surfaces [25]. In this case a linear correlation between the C–O stretching frequencies $\bar{\nu}$ and the square root of the overlap population P has been obtained.

In this paper we calculate the shift of the observed IRRAS band as a function of both the degree of CO surface coverage θ_{CO} and the applied electric potential at either the metal–vacuum interface (UHV) or the metal–solution interface (electrochemical media). The calculations are performed for the following surfaces: Pt(111), Pt(110) and Rh(111). The frequency shift of the internal modes of CO can be determined by different effects [26] such as mechanical renormalization, chemical interaction among the metal and other adsorbed molecules and self-image effects. The present calculations are focused on the shift induced by the chemical interaction.

The following topics are covered in this paper. First, the spectroscopic data for CO adsorbed at the metal–vacuum and metal–solution interfaces are summarized. Next the calculation procedure is outlined, and a correlation between the experimental frequency of CO and the calculated overlap population between the C and O atoms of the CO molecule is established. The shifts in the stretching frequency of adsorbed CO calculated for different conditions (surface coverage, applied potential etc.) are compared with the experimental data. Finally, a molecular orbital interpretation is applied to the stretching frequency shift of CO based on a population analysis of the CO molecular orbitals.

SUMMARY OF THE SPECTROSCOPIC DATA FOR ADSORBED CO AT THE METAL–VACUUM AND THE METAL–SOLUTION INTERFACES

The vibrational spectra of CO adsorbed on the Pt(111) and Pt(110) surfaces have been extensively investigated using both IRRAS and electron emission loss spectroscopy (EELS) [27] under UHV conditions. The corresponding electrochemical interface has been the subject of similar research [4,5,14–16].

TABLE 1

Summary of the experimental stretching frequencies ν_{CO} of CO reported in the literature for the adsorption of CO on different crystalline surfaces

Surface	Media	ν_{CO}^{exp}/cm^{-1}	θ_{CO}	Reference
Pt(111)	UHV	2085	0.1	[16]
		2095	0.5	
		2110	0.65	
	Solution	2056	0.2	
	0 V/SCE	2066	0.6	
Rh(111)	UHV	2015	0.05	[14]
		2065	0.75	
	Solution	2033	0.25	
	0.2 V/SCE	2041	0.75	
	pH 1			
	Solution	2015	0.70	
	0.2 V/SCE			
Pt(110)	UHV	2080	0.1	[16]
		2117	0.9	
	Solution	2063	0.1	
	0 V/SCE	2074	$\simeq 1$	

When CO is adsorbed on a metal surface in UHV, two C–O stretching adsorption bands are observed. At low θ_{CO} a band in the 2000–2100 cm^{-1} range is observed, but as θ_{CO} increases this band shifts to higher wave numbers and its intensity increases. When θ_{CO} approaches monolayer coverage by CO adsorbate the band is located at 2100 cm^{-1} [14]. At intermediate values of θ_{CO}, a second band at about 1850 cm^{-1} can be seen. This band exhibits the same characteristics as those of the preceding band when θ_{CO} is increased [14]. Comparison of these data with those obtained from metal carbonyl complex spectra and LEED patterns allows assignment of the 2100 cm^{-1} band to the C–O stretching mode of linear adsorbed CO and the 1850 cm^{-1} band to multibonded CO adsorbates [14,15].

Similarly to spectra for the metal–gas interface, the IRRAS spectrum of CO adsorbates on Pt electrodes also presents two bands, one in the range 2000–2100 cm^{-1} and the other at ca. 1800 cm^{-1}. By analogy with the spectra derived under UHV, the band at ca. 2050 cm^{-1} can be assigned to linearly bonded CO adsorbates and the band at 1800 cm^{-1} to multibonded CO [16].

As the applied electric potential is increased positively, the C–O stretching band shifts to higher frequencies. A reasonable linear relationship between the applied electric potential and the C–O stretching frequency is observed for Pt(111) single-crystal surfaces [15,16]. In this respect, no experimental data are available for Pt(110) and Rh(111).

Table 1 shows a summary of the values of ν_{CO} reported in the literature for the adsorption of CO on different crystalline surfaces and for different interfaces and degrees of surface coverage.

THE CALCULATION PROCEDURE

Following previously reported procedures [21], we can determine the vibration frequency of adsorbed CO by taking the calculated C–O overlap populations as a measure of the C–O force constant. The force constant can then be related to the vibrational frequencies. The value of the overlap population P_{ab} between atoms a and b is defined as

$$P_{ab} = \sum_i \sum_{j_a} \sum_{j_b} N_i C_{ij_a} C_{ij_b} \int \phi_{j_a} \phi_{j_b} \, d\tau \tag{1}$$

where N_i is the occupation number of orbital i.

For the calculation of wave functions of the Me-adsorbed CO system, we used a modified version of EHMO, known as the ASED-MO technique [28], to calculate the wavefunctions of the Me-adsorbed CO system. The procedure has been described in ref. 9. For clarity, the method is briefly described below.

In this method, the total energy E_{TOT} is calculated by the summation of an attractive and repulsive energy:

$$E_{TOT} = E_{ATT} + E_{REP} \tag{2}$$

The repulsive energy E_{REP} is an approximate expression derived from an analysis of corrections due to electron–electron interactions. We use the approximation proposed by Anders et al. [29] for E_{REP}. The attractive energy E_{ATT} is found by applying EHMO techniques.

The matrix elements of the attractive component of the energy are calculated from the following equations:

$$\begin{aligned} H_{ii}^{aa} &= -(\mathrm{VSIP})_i^a \\ H_{ij}^{aa} &= 0 \\ H_{ij}^{ab} &= 1.125\left(H_{ii}^{aa} + H_{jj}^{bb}\right) S_{ij}^{ab} \exp(-0.13R) \end{aligned} \tag{3}$$

where i runs over all orbitals and a runs over all atoms, VSIP stands for the valence state ionization potential, S_{ij}^{ab} is the overlap integral between orbital i on centre a and orbital j on centre b, and R is the internuclear distance between centres a and b. The exponents ζ of the Slater orbitals were taken from the literature [30]. Table 2 summarizes the values of the parameters VSIP and ζ used throughout the present calculations. These values correspond to the zero-potential condition.

The application of positive electric potentials to the interface was simulated by decreasing the VSIP values of Me (Me = Pt, Rh) from the reference value listed in Table 2. As already determined in earlier work [9], a 1 V shift in the applied electric potential corresponds to a 0.3 eV shift in the VSIP.

The $[Me(111)]_{22}$ and $[Me(110)]_{25}$ clusters, which have their d bands filled with at least one electron per orbital, have been used to model the single crystal metal surfaces throughout the present study (Fig. 1). The clusters were constructed

TABLE 2

Parameters used in the calculations: principal quantum number n for s, p and d orbitals, orbital exponent ξ, ionization potential VSIP and coefficients C_1 and C_2 for the d orbitals

Atom	s			p			d					
	n	ξ	VSIP	n	ξ	VSIP	n	ξ_1	VSIP	C_1	C_2	ξ_2
O [a]	2	2.146	−26.98	2	2.127	−12.12						
C [a]	2	1.658	−18.50	2	1.618	−9.760						
Pt [b]	6	2.550	−10.72	6	2.250	−6.725	5	6.010	−11.32	0.6640	0.5779	2.390
Pt [c]	6	2.850	−10.99	6	2.550	−6.995	5	6.310	−11.59	0.6640	0.5779	2.410
Rh [b]	5	2.135	−9.17	5	2.100	−5.814	4	4.290	−11.27	0.5807	0.5685	1.970
Rh [c]	5	2.435	−9.67	5	2.400	−6.314	4	4.590	−11.77	0.5807	0.5685	2.270

[a] Atom in CO molecule.

[b] Me in $[Me]_N(CO)$ ensembles.

[c] Me in $[Me]_N(OH)_n(CO)_m$ ensembles.

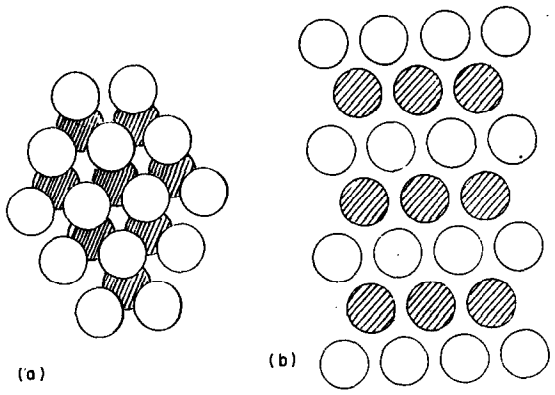

Fig. 1. Clusters used to model (a) the Pt(111) and Rh(111) surfaces, and (b) the Pt(110) surface.

geometrically from the distances of closest approach of Rh–Rh and Pt–Pt, i.e. 2.687 Å and 2.770 Å respectively.

The smallest cluster dimension compatible with the minimum influence of border effects was used when modelling the adsorption systems. Accordingly, interactions between adsorbates on the four central atoms of the cluster have been calculated. The equilibrium distances of Me–CO, O–H and C–O were calculated from the minima of the energy versus bond length curves. The corresponding values are summarized in Table 3.

CORRELATION BETWEEN THE EXPERIMENTAL STRETCHING FREQUENCY AND THE OVERLAP POPULATION

Many theoretical calculations correlating macroscopic properties of adsorbed CO on metal surfaces and the overlap population of CO have been published. Politzer and Kasten [21] used the charge iterative form of EHMO theory including Madelung repulsions and Cusach's approximation to estimate vibrational frequencies of CO chemisorbed on an $[Ni(100)]_q$ cluster. These authors prepared a calibration curve by plotting the calculated total C–O overlap populations for isolated CO, CO^+, $Ni(CO)_4$ and H_2CO molecules versus the C–O force constants derived from spectroscopic measurements. The resulting function was sigmoidal rather than linear. By interpolation of this calibration curve, they used computed C -O overlap populations of adsorbed CO molecules on their clusters to estimate

TABLE 3

Calculated equilibrium distances for metal–CO, C–O and O–H bonds

	Pt–CO	Rh–CO	C–O	O–H
Distance Å	2.05	2.0	1.16	1.0

values of the force constant k_e for each adsorbed molecule. Finally, the C–O stretching frequencies were calculated using the harmonic oscillator approximation.

Schreiner and Brown [31] have found, using EHMO calculations for the metal carbonyl complexes $Ni(CO)_4$, $Cr(CO)_6$ and $Fe(CO)_5$, a linear relationship between M–C overlap population and M–CO dissociation energies (which are frequently considered to be related to force constants).

Kusuma and Companion [25] used EHMO theory in the investigation of CO/Ni(111) systems. They studied the preferred orientation of the CO molecule in the presence of coadsorbed neighbours and the stability of clusters of CO, H and O. They obtained monotonic calibration curves between the experimental stretching frequencies of several metal carbonyls and their computed C–O overlap populations. These correlations were then used to predict the stretching frequency of a CO molecule adsorbed on an Ni(111) surface in the presence of other CO molecules, H atoms and O atoms.

Following the methodology described earlier in this section, we shall analyse here the correlation between the experimental frequency ν_{CO}^{exp} of CO adsorbed on a Pt(111) single-crystal surface and the square root of the CO overlap population P_{CO} calculated according to eqn. (1). Experimental ν_{CO}^{exp} values were taken from the IRRAS data of Chang and Weaver [15]. They obtained a linear relation between ν_{CO}^{exp} and the applied electric potential V at different values of θ_{CO} as shown in Fig. 2(a). The data in this figure can also be presented as shown in Fig. 2(b) in which the values of the ν_{CO}^{exp} are plotted versus θ_{CO}; the applied electric potential is the parameter in this case. The calibration curves of $\sqrt{P_{CO}}$ vs. ν_{CO}^{exp} can be obtained using either of the two methods discussed below.

One approach is to calculate $\sqrt{P_{CO}}$ for different θ_{CO} at a given potential (i.e. $V = 0.0$ V as shown by the broken line in Fig. 2(a)) and the other is to calculate $\sqrt{P_{CO}}$ for different V at a given θ_{CO} (i.e. $\theta_{CO} = 0.33$ as shown by the broken line in Fig. 2(b)). When the values of $\sqrt{P_{CO}}$ calculated using the two approaches are

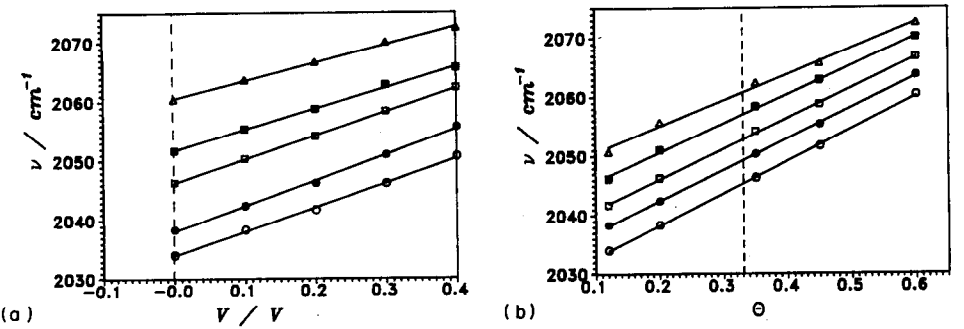

Fig. 2. (a) Experimental correlation between ν_{CO} and the applied electric potential [15]: ○ $\theta_{CO} = 0.12$; ● $\theta_{CO} = 0.20$; □ $\theta_{CO} = 0.35$; ■ $\theta_{CO} = 0.45$; △ $\theta_{CO} = 0.60$. (b) Experimental correlation between ν_{CO} and θ_{CO} derived from (a): ○ $V = 0.0$ V; ● $V = 0.1$ V; □ $V = 0.2$ V; ■ $V = 0.3$ V; △ $V = 0.4$ V.

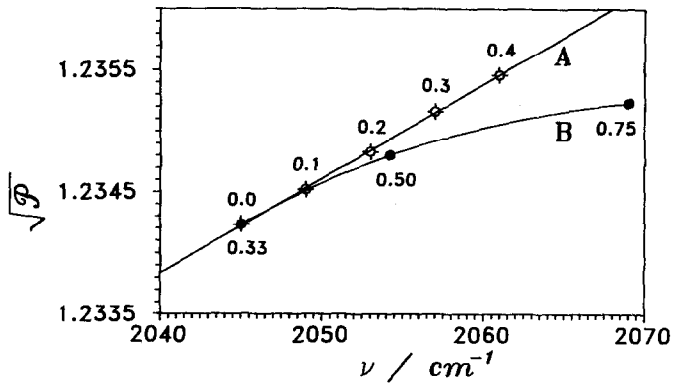

Fig. 3. Correlation between the theoretical $\sqrt{P_{CO}}$ calculated in the present work and the experimental CO stretching frequencies ν_{CO} [15].

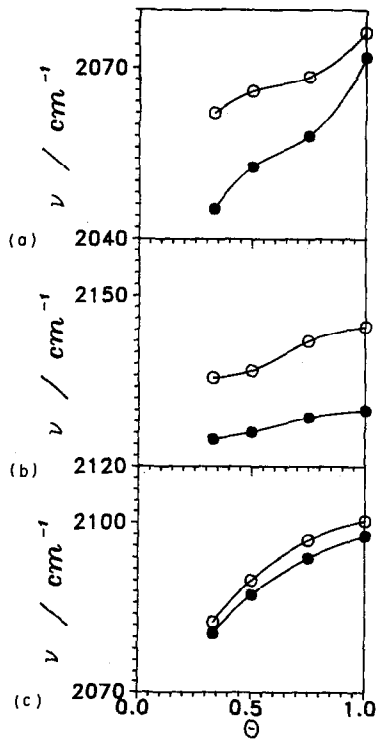

Fig. 4. Theoretical dependence of ν_{CO} on θ_{CO} for the Me–CO(vacuum) (○) and the Me–CO(solution) (●) interfaces (electrode potential, 0 V/SHE): (a) Pt(111); (b) Pt(110); (c) Rh(111).

plotted versus ν_{CO}^{exp} we obtain the curves shown in Fig. 3. Curve A is the result of the second approach with $\theta_{CO} = 0.33$. The values of V are indicated in the figure. From a linear least squares fit of the data we obtain

$$\sqrt{P_{CO}} = 1.0757 + 7.75 \times 10^{-5}\ \nu_{CO}^{exp}/cm^{-1} \quad (4)$$

with a correlation factor of $\rho = 0.9998$. Curve B was obtained for a fixed applied potential (0 V). The θ_{CO} values are indicated in the figure. It can be seen that the relation between $\sqrt{P_{CO}}$ and ν_{CO}^{exp} is parabolic rather than linear.

Curves A and B should overlap since the relation between $\sqrt{P_{CO}}$ and ν_{CO}^{exp} should be a universal function. However, some deviation of curve B from linearity should be expected since surface coverages are not well defined for our small clusters, in particular for high θ_{CO}. Figure 3 shows that the curves overlap for low values of θ_{CO}, while this is not the case for higher values.

RESULTS

In this section we compare the ν_{CO}^{exp} values with those calculated using eqn. (4) and following the procedures described in the preceding section. We shall analyse

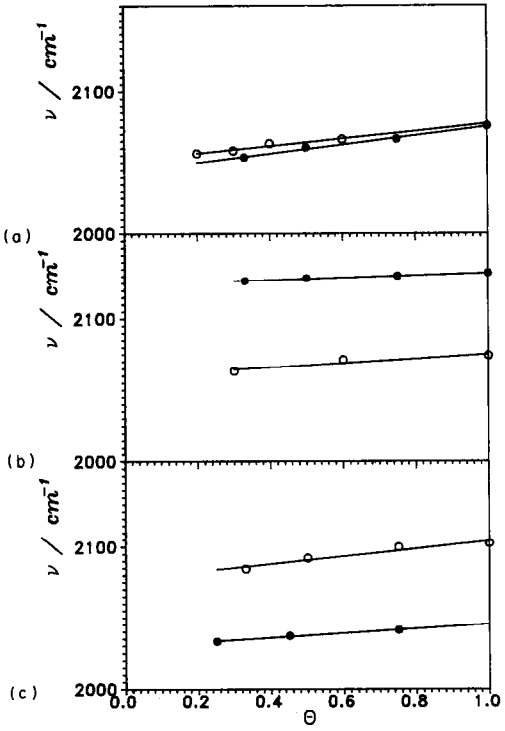

Fig. 5. Theoretical (●) and experimental (○) ν_{CO} vs. θ_{CO} plots for the Me–CO(solution) electrochemical interface: (a) Pt(111) in 0.1 M $HClO_4$ at 0.0 V/SCE; (b) Pt(110) in 0.1 M $HClO_4$ at 0.0 V/SCE; (c) Rh(111) at pH 1 at 0.2 V/SCE.

the variation of ν_{CO} with the applied electric potential, the surface coverage and the topology and nature of the surface.

We obtained a value of 2145 cm^{-1} for the stretching frequency of a free CO molecule. After CO adsorption (metal–vacuum interface) this value changes to 2061 cm^{-1} for $[Pt(111)]_{22}$, 2123 cm^{-1} for $[Pt(110)]_{25}$ and 1930 cm^{-1} for $[Rh(111)]_{22}$. These results are in agreement with the experimental results reported in the literature (see section describing the summary of spectroscopic data).

The variation of the calculated ν_{CO} with θ_{CO} is shown in Fig. 4. The calculation was performed for the Me–CO(vacuum) and Me–CO(solution) interfaces, and the values of θ_{CO} are in the range 0.33–1 for the Pt(111) (Fig. 4(a)), Pt(110) (Fig. 4(b)) and Rh(111) (Fig. 4(c)) surfaces.

The calculated values of ν_{CO} for the Pt(111)–CO(vacuum) interface at 0.0 V increase from 2062 to 2068 cm^{-1} when θ_{CO} is increased from 0.33 to 1. For the Pt(110) surface, ν_{CO} changes from 2124 cm^{-1} to 2143 cm^{-1} for the same increase in the surface coverage, and in the case of Rh(111) the change is from 2080 to 2096 cm^{-1}. The presence of the aqueous environment results in a diminution of ν_{CO}

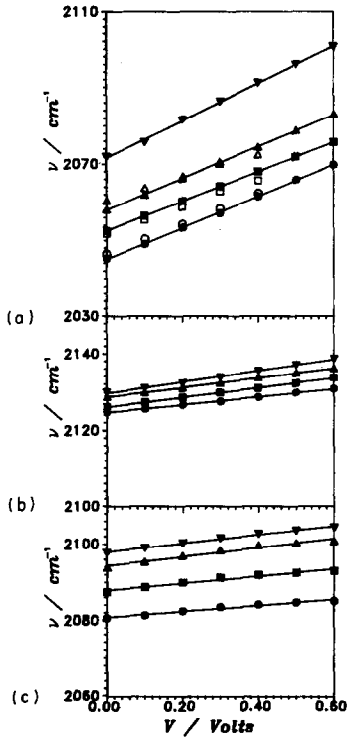

Fig. 6. ν_{CO} versus applied electric potential for different values of θ_{CO}: (a) Pt(111); (b) Pt(110); (c) Rh(111). Theoretical calculations: ● $\theta_{CO} = 0.33$; ■ $\theta_{CO} = 0.5$; ▲ $\theta_{CO} = 0.75$; ▼ $\theta_{CO} = 1$. Experimental results [15]: ○ $\theta_{CO} = 0.35$; □ $\theta = 0.45$; △ $\theta = 0.60$.

with respect to the values observed for the Me–CO(vacuum) interface. As in the case of the metal–vacuum interface, ν_{CO} increases with θ_{CO}. For Pt(111) the variation of ν_{CO} is 26 cm^{-1} when θ_{CO} changes from 0.33 to 1. For Pt(110) the variation is 5.4 cm^{-1} and for Rh(111) it is 17 cm^{-1} under the same conditions.

Figure 5 shows the experimental and calculated values of ν_{CO} obtained under identical conditions for different monocrystalline surfaces in the aqueous environment. The agreement between the experimental and theoretical values is excellent in the case of Pt(111), while for the other surfaces it is similar to that obtained with ab-initio calculations [20,24].

The variation of ν_{CO} with the applied electric potential is shown in Fig. 6. A linear relation between ν_{CO} and V is obtained for the different surfaces. For Pt(111) (Fig. 6(a)) we have also plotted experimental values taken from ref. 15. As can be seen, very good agreement is obtained between theory and experiment.

DISCUSSION

The changes in ν_{CO} with the adsorption of CO on a metallic surface, when the surface coverage increases or when the nature of the interface changes and an electric field is applied can be explained by applying molecular orbital (MO) theory to adsorbed CO. The nature of the CO–metal interaction and, in particular, the changes in ν_{CO} for CO adsorbed on different sites can be rationalized on the basis of a simple MO model which postulates a σ charge donation from the CO to the metal and mixing of the metal orbitals with the π orbitals of CO (Blyholder model). This basic picture of σ donation and π backbonding has been used by inorganic chemists and later extended to surface chemistry. The relative importance of the σ and π bonding contributions undoubtedly varies from metal to metal and from one site to another on a particular metal [24].

Thus in order to obtain a deeper insight into the nature of the chemical bonds involved in the adsorption of CO on the different metal surfaces, we performed a population analysis of the projection of the MOs of $[Me]_N(CO)_M$ and $[Me]_N(OH)(CO)_M$ clusters onto the MOs of the free CO molecule. This approach is very useful since the extent to which each MO of free CO participates in the CO–metal bond can be inferred from analysis of the changes in the population of each MO.

Table 4 shows the Mülliken population analysis for a free CO molecule and for a CO molecule adsorbed on different sites of a Pt(111) surface. This analysis shows that the 5σ and $2\pi^*$ MOs and, to a lesser extent, the 4σ MO of CO participate in the chemical bond between CO and the metal surface. There is a charge transfer from the CO MO into the metal and back-donation from the metal d band to the unoccupied $2\pi^*$ orbital of CO. Thus the population of the 5σ MO of the free CO diminishes by approximately 30% and that of the 4σ MO diminishes by about 10%. Part of the total charge is transferred to the CO $2\pi^*$ MO by the metal and the rest is transferred to the metal. This causes the CO bond to weaken as a

TABLE 4

MO populations for free CO and for CO adsorbed on different sites on a Pt(111) surface

Orbital	Free CO	Top CO	Bridge CO	Hollow CO
$2\pi^*$	0.0	0.1973	0.5312	0.5337
5σ	2.0	1.4103	1.4013	1.3525
2π	4.0	3.9998	3.9476	3.9463
4σ	2.0	1.8246	1.7797	1.8016
3σ	2.0	2.0020	2.0118	2.0119
Total charge	10.0	9.4340	9.6716	9.6460

consequence of back-donation into the $2\pi^*$ MO which leads to the lowering of the CO stretching frequency discussed earlier.

The experimental ν_{CO} for adsorption on different sites decreases in the order top > bridge > hollow. This trend is confirmed by our population analysis for the different MOs. Thus, the $2\pi^*$ MO population gives 0.1973, 0.5312 and 0.5337 for the top, bridge and hollow sites respectively (Table 4), whereas the 5σ MO population decreases in the same order.

It has already been shown that ν_{CO} increases with θ_{CO}. This trend is due to two simultaneous effects: the direct CO–CO interaction and the CO–metal–CO interaction. In order to analyse the former, we performed a population analysis of "CO clusters" of the same geometry as those observed on the metallic surface but without the metal substrate. The results are shown in Table 5. It can be seen that the CO–CO interaction (in the absence of the metal) leads to an increase in the $2\pi^*$ MO population and a decrease in the 5σ MO population. This indicates that in a "pure CO" cluster the CO bond is weakened, which would produce a decrease in ν_{CO}. Since this result disagrees with that obtained when the metal is present (Figs. 4 and 5), we can conclude that the direct CO–CO interaction is not the predominant effect in the changes of ν_{CO} with θ_{CO}. However, when CO is adsorbed on a metal surface, further adsorption of other CO molecules increases

TABLE 5

MO populations for different "pure CO" clusters

Orbital	$\theta_{CO} = 0.33$	$\theta_{CO} = 0.50$	$\theta_{CO} = 0.75$	$\theta_{CO} = 1.0$
$2\pi^*$	0.0	0.0	0.023	0.024
5σ	2.0	2.0	1.988	1.979
2π	4.0	4.0	4.000	4.000
4σ	2.0	2.0	1.989	1.997
3σ	2.0	2.0	2.000	2.000
Total charge	10.0	10.0	10.000	10.000

θ_{CO} is the degree of surface coverage that would be attained if the molecules were adsorbed on the substrate surface.

TABLE 6

MO populations for CO adsorbed on a Pt(111) surface at different surface coverages

Orbital	$\theta_{CO} = 0.33$	$\theta_{CO} = 0.50$	$\theta_{CO} = 0.75$	$\theta_{CO} = 1.0$
Metal–CO(vacuum) interface				
$2\pi^*$	0.1973	0.1957	0.1917	0.1895
5σ	1.4103	1.4109	1.4123	1.4175
2π	3.9998	3.9988	3.9980	3.9980
4σ	1.8246	1.8232	1.8226	1.8224
3σ	2.0020	2.0030	2.0050	2.0070
Total charge	9.4340	9.4316	9.4305	9.4344
Metal–CO(solution) interface				
$2\pi^*$	0.1883	0.1997	0.2007	
5σ	1.4109	1.4117	1.4255	
2π	3.9880	3.9910	3.9910	
4σ	1.8229	1.8229	1.8230	
3σ	2.0020	2.0030	2.0050	
Total charge	9.4121	9.4283	9.4452	

the bonding of the 5σ MO population, leaving the $2\pi^*$ population almost unchanged. Thus the net effect is a strengthening of the CO bond which implies an increase in ν_{CO}.

As shown above, the value of ν_{CO} depends on the nature and topology of the metal surface. This is also reflected in a population analysis. For Pt(111) [Pt: d^9s^1] we obtained a population of 0.2124 for the $2\pi^*$ MO and 1.4552 for the 5σ MO, while for Rh(111) [Rh: d^8s^1] the corresponding populations are 0.2272 and 1.4692 respectively. These changes imply that $\nu_{CO-Pt} > \nu_{CO-Rh}$ as observed experimentally and as calculated in the previous section. Concerning the topology of the surface, we recall that a higher value of ν_{CO} was obtained for the less compact Pt(110) surface than for the Pt(111) surface. The population of the $2\pi^*$ MO for Pt(110) is 0.1671 while for Pt(111) it is 0.2272. Thus the fact that the Pt(110) surface has the highest ν_{CO} is also related to the low population of its $2\pi^*$ MO. The populations of the 5σ MOs are 1.4552 and 1.3293 for the Pt(111) and Pt(110) surfaces respectively.

The presence of the aqueous environment produces a decrease in ν_{CO} values relative to those observed for the metal–vacuum interface. The adsorption of water and/or its decomposition products such as OH^- modify the charge-transfer mechanism of the Me–CO system. As can be seen in Table 6, both the $2\pi^*$ and 5σ population increase. However, since the 5σ MO implies only weak bonding and, the $2\pi^*$ MO is strongly antibonding, the CO bond is weakened and the increase of the back-donation into the $2\pi^*$ orbital results in a drastic diminution of ν_{CO}.

Finally, we analyse the influence of the electric potential V applied to the metal–solution interface. As can be seen in Table 7, as the applied potential

TABLE 7

MO populations for CO adsorbed on a Pt(111) surface at different applied electric potentials

Orbital	Metal–CO(solution) interface		
	$V = 0.1$	$V = 0.2$	$V = 0.3$
$2\pi^*$	0.1975	0.1902	0.1834
5σ	1.4090	1.3989	1.3887
2π	3.9921	3.9916	3.9907
4σ	1.8218	1.8191	1.8161
3σ	2.0027	2.0029	2.0026
Total charge	9.4230	9.4027	9.3816

$\theta_{CO} = 0.33$ in all cases.

increases the $2\pi^*$ and 5σ MO populations decrease linearly which implies an increase in the charge transfer to the metal. This is reflected by an increase in ν_{CO}.

CONCLUSIONS

On the basis of experimental results reported in the literature for the variation of ν_{CO} with factors such as θ_{CO}, applied electric potential and environment, we have obtained a linear correlation between measured macroscopic properties (ν_{CO}) and quantum calculations ($\sqrt{P_{CO}}$). Using the linear correlation found between ν_{CO} and $\sqrt{P_{CO}}$ we calculated the changes in ν_{CO} induced by changes in the applied potential, the surface coverage and the nature of the surface itself. The calculations are in reasonable agreement with the experimental results. The population analysis performed indicates that the variation in ν_{CO} can be explained in terms of the donation–back-donation model.

ACKNOWLEDGEMENTS

This work was supported by the Consejo de Investigaciones Científicas y Tecnológicas de la Provincia de Córdoba (CONICOR), the Consejo Nacional de Investigaciones Científicas y Técnicas, the Secretaria de Ciencia y Tecnologia de la Universidad Nacional de Córdoba and Fundación Antorchas, Argentina. Language assistance from P. Falcon is also acknowledged. P.P.O. thanks CONICOR for a fellowship.

REFERENCES

1 B. Beden, A. Bewick, K. Kunimatsu and C. Lamy, J. Electroanal. Chem., 114 (1984) 3434.
2 J. Léger, B. Beden, C. Lamy and S. Bilmes, J. Electroanal. Chem., 170 (1984) 305.
3 F. Kitamura, M. Takahashi and M. Ito, J. Phys. Chem., 92 (1988) 3320.
4 L. Leung, A. Wieckowski and M.J. Weaver, J. Phys. Chem., 92 (1988) 6985.
5 S.G. Sun, J. Clavilier and A. Bewick, J. Electroanal. Chem., 257 (1988) 147.

6 E. Santos, E.P.M. Leiva, W. Vielstich and U. Linke, J. Electroanal. Chem., 227 (1987) 199.
7 R. Parsons and T. VanderNoot, J. Electroanal. Chem., 257 (1988) 9.
8 K. Kunimatsu, J. Electroanal. Chem., 213 (1986) 149.
9 P. Paredes Olivera, G. Estiú, E.A. Castro and A.J. Arvia, J. Mol. Struct., 210 (1990) 393.
10 P. Paredes Olivera, G. Estiu, E.A. Castro and A.J. Arvia, to be published.
11 S.C. Chang and M.J. Weaver, J. Electroanal. Chem., 285 (1990) 263.
12 J.W. He, W.K. Kuhn, L.W. Leung and D.W. Goodman, J. Chem. Phys., 93 (1990) 7463.
13 B. Beden, Spectroscopic and Diffraction Techniques in Interfacial Electrochemistry, Kluwer, 1990, p. 103.
14 L.W. Leung, S.C. Chang and M.J. Weaver, J. Chem. Phys., 90 (1989) 7426.
15 S.C. Chang and M.J. Weaver, J. Chem. Phys., 92 (1990) 4582.
16 S.C. Chang, L.W. Leung and M.J. Weaver, J. Phys. Chem., 93 (1989) 5341.
17 P.S. Bagus, C.J. Nelin, W. Müller, M.R. Philpott and H. Seki, Phys. Rev. Lett., 58 (1987) 559.
18 G. Pacchioni and P. Bagus, J. Chem. Phys., 93 (1990) 1209.
19 P. Bagus and G. Pacchioni, Surf. Sci., 236 (1990) 1209.
20 N. Rösch, A. Görling, P. Knappe and J. Lauber, Vacuum, 41 (1990) 1.
21 P. Politzer and S.D. Kasten, J. Phys. Chem., 80 (1976) 385.
22 S. Holloway and J. Norskov, J. Electroanal. Chem., 161 (1984) 193.
23 A. Anderson, R. Kötz and E. Yeager, Chem. Phys. Lett., 82 (1981) 131.
24 G. Blyholder and H. Sellers in G. Pachioni and P.S. Bagus (Eds.), Cluster Models of Surface and Bulk Phenomena, Plenum Press, New York, 1991.
25 T. Kusuma and A. Companion, Surf. Sci., 195 (1988) 59.
26 F. Hoffman, Surf. Sci. Rep., 3 (1983) 107.
27 J.T. Yates Jr and T.E. Madey, Vibrational Spectroscopy of Molecules on Surfaces, Plenum Press, New York, 1987.
28 A. Anderson, R. Grimes and S.Y. Hong, J. Phys. Chem., 91 (1987) 4245.
29 L.W. Anders, R. Hansen and L. Bartell, J. Chem. Phys., 59 (1973) 5277.
30 E. Clementi and C. Roetti, Atomic Data and Nuclear Data Tables, Vol. 14, Academic Press, New York, 1974.
31 A.F. Schreiner and T.L. Brown, J. Am. Chem. Soc., 90 (1968) 3366.